Analysis of the Polarization of a Single-Mode VCSEL Subject to Parallel Optical Injection

Quirce, Ana; Popp, Alexandra; Denis-Le Coarer, Florian; Perez, Pablo; Valle, Angel; Pesquera, Luis; Hong, Yanhua; Thienpont, Hugo; Panajotov, Krassimir; Sciamanna, Marc

Journal of the Optical Society of America B: Optical Physics

DOI:
10.1364/JOSAB.34.000447

Published: 01/02/2017

Peer reviewed version

Analysis of the Polarization of a Single-Mode VCSEL Subject to Parallel Optical Injection

ANA QUIRCE[1], ALEXANDRA POPP[2], FLORIAN DENIS-LE COARER[2,3,*], PABLO PÉREZ[2], ÁNGEL VALLE[2], LUIS PESQUERA[2], YANHUA HONG[4], HUGO THIENPONT[1], KRASSIMIR PANAJOTOV[1,5], AND MARC SCIAMANNA[3,6]

[1] *Vrije Universiteit Brussel, Faculty of Engineering Sciences, Brussels Photonics Team B-PHOT, Pleinlaan 2, 1050, Brussels,Belgium.*
[2] *Instituto de Física de Cantabria (CSIC-Univ. Cantabria), Avda. Los Castros s/n, E39005, Santander, Spain.*
[3] *OPTEL Research Group, LMOPS laboratory, CentraleSupélec, University of Paris-Saclay, and University of Lorraine, 57070 Metz.*
[4] *School of Electronic Engineering, Bangor University, Gwynedd LL57 1UT, Wales, UK*
[5] *Institute of Solid State Physics, 72 Tzarigradsko, Chaussee Blvd., 1784 Sofia, Bulgaria.*
[6] *OPTEL Research Group, LMOPS laboratory, Université de Lorraine, 57070, Metz, France*
[*] *Corresponding author: florian.denis@supelec.fr*

We investigate experimentally and theoretically the polarization switching found in a single-transverse mode VCSEL when subject to parallel optical injection. Our analysis focuses on a recently observed state in which injection locking of the parallel polarization and excitation of the free-running orthogonal polarization of the VCSEL are obtained. A simple nonlinear dependence between the power of both linear polarizations and the frequency detuning is found. Also the total power emitted by the VCSEL is constant and independent on the injected optical power and on the frequency detuning. We check these results experimentally for a variety of frequency detunings and bias currents applied to the device. We report experimental and theoretical stability maps in the injected power-frequency detuning plane for different bias currents identifying the regions in which the state is observed. A simple analytical expression that describes the map boundary for large and negative frequency detunings is obtained. This provides a simple method to extract the linear dichroism of the device.

OCIS codes: *(140.5960) Semiconductor lasers;(140.7260) Vertical-Cavity Surface-Emitting Lasers; (140,3520) Lasers, injection-locked; (190.1450) Bistability*

1. INTRODUCTION

External optical injection in semiconductor lasers has been a subject of interest for many years [1–5]. Injection locking is a technique commonly employed to improve the semiconductor laser performance. Reduction of frequency chirp, enhancement of spectral stability, suppression of laser noise, and improvement of the laser intrinsic frequency response have been reported [1–3]. Also optical injection in laser diodes is an attractive way for obtaining fast nonlinear and chaotic dynamics [3–6] with applications in microwave photonics, chaos-based secure communications, optical sensing, and random number generation [6]. Vertical-cavity surface-emitting lasers (VCSELs) are semiconductor lasers that offer inherent advantages in comparison to edge-emitting devices [7, 8]. These advantages include reduced manufacturing costs, on-wafer testing capability, high-coupling efficiency to optical fibers, ease of fabrication of 2D arrays, low threshold current, compactness and single mode operation [7, 8]. Injection locking has been used to enhance the modulation bandwidth of VCSELs [9].

Although VCSELs are intrinsically single-longitudinal mode devices, they usually show complex polarization characteristics [7, 10]. The light emitted by the VCSEL is typically linearly polarized along one of two orthogonal directions and polarization switching (PS) between the two orthogonal polarizations can be observed when temperature or bias current is changed [7]. Optical injection is also a technique used to achieve PS in VCSELs [11–18]. This has been usually obtained for the case of orthogonal optical injection: linearly polarized light from an external laser is injected orthogonally to the linear polarization of the solitary VCSEL. Very recently it has been shown experimentally and theoretically that PS in single-transverse mode VCSELs can also be obtained for parallel optical injection, that is, the directions of linear polarization of the injected light and the free-running device are parallel [19]. A state, termed as IL+PS,

in which injection locked emission in the parallel polarization and excitation of the free-running orthogonal polarization of the VCSEL occurs simultaneously was described. This is an unusual situation because optical injection in the polarization with smaller optical losses causes emission in the polarization with larger losses [19]. Very recently a linear stability analysis of the mixed-mode steady states of an optically injected two-polarization modes edge-emitting semiconductor laser has been performed [20]. Dynamical evolution of mixed-mode steady states and IL+PS states is similar for VCSELs for which the spin dynamics can be adiabatically eliminated [19], and so the linear stability analysis of [20] was successfully extended to the VCSEL case [19]. Also two-mode equilibrium state (TME) has been observed in optically injected two-mode lasers [21–23]. There are some differences with respect to our case. IL+PS is observed in a single-mode laser, however, TME was observed in a two-mode laser. Also just a single linear polarization is excited in TME, however, in IL+PS the polarization behaviour is more complex because two modes with orthogonal linear polarizations are excited.

In this work we extend the experimental and theoretical study of [19]. We study PS in a single-transverse mode VCSEL subject to parallel optical injection around the frequency of the parallel polarization mode of the free running VCSEL. We focus on the theoretical and experimental characterization of the IL+PS state for a wide range of operating conditions. **We extend the results of Ref. [19] by analyzing the dependence of IL+PS state on the device bias current and on the frequency detuning between the injected light and the parallel linear polarization of the VCSEL. Some of the theoretical results predicted in [19] are checked in this work. These include i) the simple nonlinear dependence between the power of both linear polarizations and the frequency detuning and, ii) the independence of the total emitted power on the frequency detuning. A detailed derivation of the analytical expressions describing the IL+PS state and its linear stability analysis is also given. We extend the study of Ref. [19] in order to analyse the effect of the bias current on the theoretical and experimental stability maps. We also explain how measurements of the boundaries of region in which IL+PS is observed can be used for the extraction of some parameters characterizing the polarization of the VCSEL.**

This paper is organized as follows. Section 2 gives a description of the experimental setup. In section 3 we present our experimental results. Section 4 is devoted to the description of the theoretical model. Our theoretical results are presented in section 5. Finally, in section 6, a discussion and summary are presented.

2. EXPERIMENTAL SETUP

Fig. 1 shows the all-fiber setup that has been developed to inject the light emitted by a tunable laser (TL, master laser) into the 1550 nm-VCSEL. A variable attenuator (VA) controls the level of optical power of the injected signal. The first polarization controller (PC1) is adjusted to assure the parallel optical injection configuration. Optical injection into the VCSEL is obtained by using a three-port optical circulator. Injected power is characterized by using a 50/50 coupler and a power meter (PM). A second polarization controller (PC2) is connected to a polarization beam splitter (PBS) to select the parallel and the orthogonal polarizations, which are analysed by two PMs or by a high-resolution Brillouin Optical Spectrum Analyser (BOSA, Aragon Photonics, with 10 MHz bandwidth resolution).

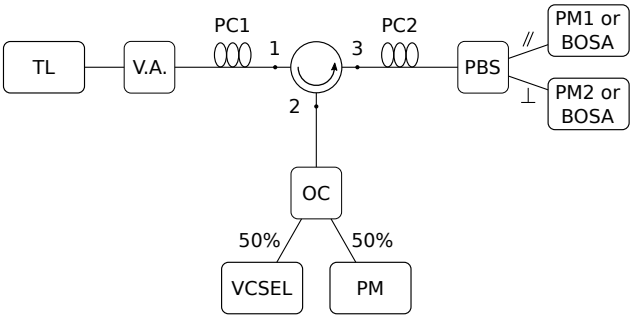

Fig. 1. Experimental setup for parallel optical injection in the VCSEL. TL: tunable laser, PC1 and PC2: polarization controllers, VA: variable attenuator, OC: optical coupler, PBS: polarization beam splitter, PM: power meter.

Our VCSEL is a long-wavelength device that emits in a single transverse mode with a threshold current of $I_{th} = 1.66$ mA at 25° C [19]. Higher-order transverse modes do not play any role in our experiment because they are highly suppressed, more than 55 dB at 3.05 mA bias current. Fig. 2 shows the optical spectrum of the free-running VCSEL at this bias current. The VCSEL emits in a linear polarization that we will call the "parallel" (or x) polarization while the orthogonal (y) polarization is shifted by 32.86 GHz toward higher frequency side [19]. The zero frequency has been chosen to correspond to the x polarization.

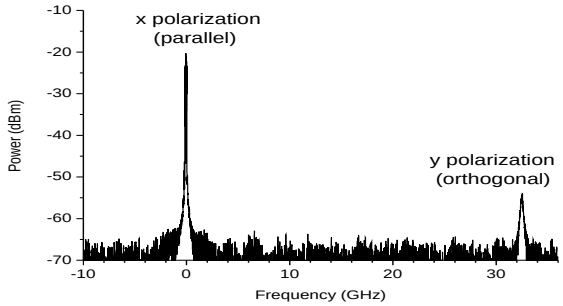

Fig. 2. Optical spectrum for the free-running VCSEL at 3.05 mA bias current.

Several PSs are observed in our solitary VCSEL for different values of the bias current: 2.25, 6.70 and 9.15 mA. These PSs are Type I, Type II, and Type I PS, respectively, where Type I PS is from the short to the long wavelength mode and Type II is the opposite. Several bias currents have been considered in our experiment. We characterize the optical injection by its strength given by the value of the power measured in front of the VCSEL, P_i, and by the frequency detuning, ν_i, defined by the difference between the injected frequency and the frequency of the lasing polarization mode of the free-running VCSEL.

3. EXPERIMENTAL RESULTS

Figure 3 shows the experimental optical spectra of both linear polarization modes as the frequency of the master laser is decreased for a fixed value of the injected power, $P_i = 65.3\ \mu$W. The bias current of the VCSEL is $I = 3.05$ mA. The observed signal is the coherent addition of the VCSEL emission and the

reflection of the optical injection from the front surface of the VCSEL. Fig. 3(a) shows a time-periodic dynamics in the parallel polarization. The self-pulsation has a 2.6 GHz frequency that is close to the relaxation oscillation frequency, 2 GHz. As we decrease ν_i we obtain injection locking in the parallel polarization as it is shown in Fig. 3(b): only one peak at the frequency of the injection appears in the optical spectrum. Further decrease of ν_i leads to PS, as shown in Fig. 3(c): the orthogonal (parallel) polarization is excited (suppressed) at its free-running frequency. Fig. 3(c) also demonstrates injection locked emission in the parallel polarization. This state was already observed in [19] and it was termed as IL+PS because injection locking of the parallel polarization and excitation of the free-running orthogonal polarization mode of the VCSEL are simultaneously obtained. Another example of IL+PS is shown in Fig. 3(d) for $\nu_i = -5.88$ GHz. This state is observed from $\nu_i = -3.38$ GHz to $\nu_i = -6.03$ GHz. Further decrease of ν_i leads to the disappearance of the orthogonal polarization with time-periodic dynamics in the parallel polarization with ν_i frequency (not shown). **The analysis of Fig. 3 complements that of Ref. [19] in which optical spectra for different injected powers, but for a fixed frequency detuning, are shown. Fig. 3(c) and Fig. 3(d) also illustrate polarization switching because optical spectra for both linear polarizations are plotted in contrast to Fig. 1. of Ref.[19] in which only optical spectra of the total power are shown.**

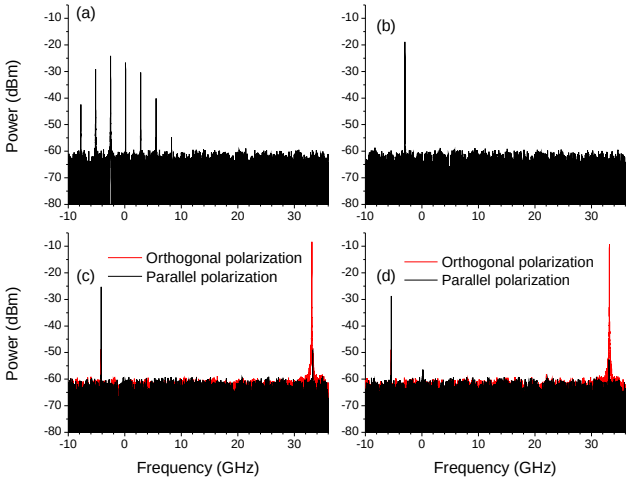

Fig. 3. Experimental optical spectra when $P_i = 65.3$ μW and $I = 3.05$ mA for different frequency detunings (a) $\nu_i = -0.59$ GHz, (b) $\nu_i = -3.27$ GHz, (c) $\nu_i = -4.74$ GHz, (d) $\nu_i = -5.88$ GHz. Black (red) colour represents the parallel (orthogonal) polarization.

We now focus on the IL+PS state. We have measured the power emitted by the VCSEL in the x, $\mathbf{P_x}$, and y, $\mathbf{P_y}$, polarizations as a function of P_i for fixed values of the bias current, I, and ν_i using the procedure explained in [19]. Fig. 4 shows our results for the cases in which IL+PS is observed, including also the values of the total power, $\mathbf{P_{tot}} = \mathbf{P_x} + \mathbf{P_y}$. Fig. 4(a) shows the results when $I = 3.05$ mA and $\nu_i = -5$ GHz. IL+PS solution is observed when 46 μW $< P_i <$ 246 μW. $\mathbf{P_x}$ and $\mathbf{P_y}$ depend linearly on P_i while $\mathbf{P_{tot}}$ is almost constant. The same behaviour is observed for a variety of bias current and ν_i values, as it is shown in Fig. 4(b)- Fig. 4(c).

Comparison between Fig. 4(a) and Fig. 3 in [19] shows that,

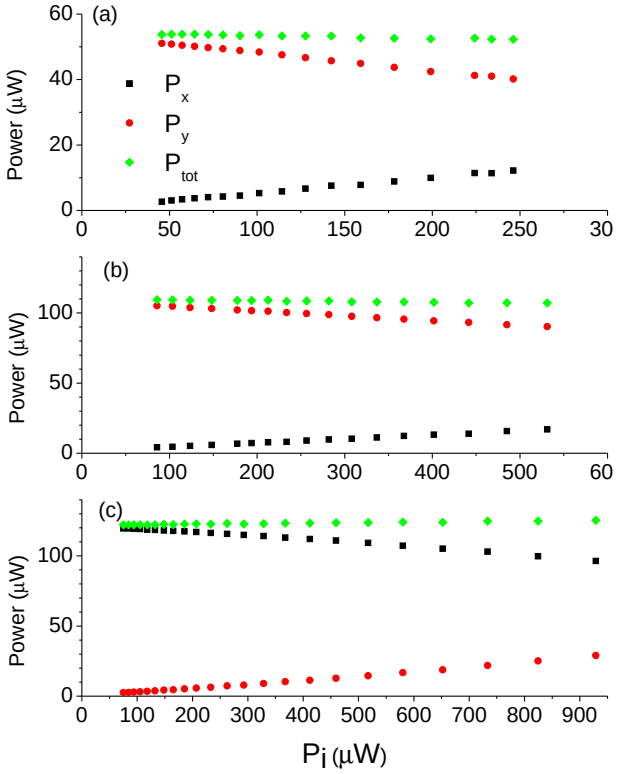

Fig. 4. Experimental values of the power of x-polarization ($\mathbf{P_x}$), of y-polarization ($\mathbf{P_y}$) and of the total power ($\mathbf{P_{tot}}$) as a function of P_i when (a) $I = 3.05$ mA, $\nu_i = -5$ GHz, (b) $I = 6$ mA, $\nu_i = -6.1$ GHz, (c) $I = 7$ mA, $\nu_i = -5.1$ GHz.

for negative ν_i values, IL+PS is observed in a narrower P_i range as ν_i approaches zero. IL+PS is also observed for some positive ν_i values. For instance when $\nu_i = 1.7$ GHz IL+PS appears if 1.5 μW $< P_i <$ 8 μW (not shown). Fig. 4(b) shows results for a larger bias current value, 6 mA. $\mathbf{P_x}$, $\mathbf{P_y}$, and $\mathbf{P_{tot}}$ are larger than the values obtained for smaller I, but their qualitative dependence on P_i is similar. Fig. 4(c) shows the results obtained when I is larger than the value at which the solitary VCSEL has PS, 6.7 mA. Now the free-running VCSEL is emitting in the y-polarization and so the direction of the optical injection is changed in order to match the y-direction. Also ν_i, -5.1 GHz, is measured with respect to the y-polarization mode frequency. Results are similar to those obtained before but exchanging the roles of x and y polarizations because now the PS induced when increasing P_i is towards the x-polarization mode. **We note that Fig. 4 illustrates how curves of Fig. 3 of Ref. [19] change when the frequency detuning and/or bias current change, results that were not included in that reference.**

We now focus on the dependence of the IL+PS state on the frequency detuning. Fig. 5 shows $\mathbf{P_x}$, $\mathbf{P_y}$, and $\mathbf{P_{tot}}$ as a function of ν_i for fixed values of P_i and I only for cases in which IL+PS is observed. Our measurements are obtained by decreasing the optical frequency of the tunable laser for $P_i = 151$ μW. Both $\mathbf{P_x}$, and $\mathbf{P_y}$ show a nonlinear dependence on ν_i in such a way that $\mathbf{P_x}$ ($\mathbf{P_y}$) increases (decreases) as ν_i approaches the zero value. Also, as in our previous results, Fig. 5(b) shows that the total power is constant, independent on ν_i.

We now characterize the region of parameters space in which the IL+PS solution is observed. Experimentally, for a fixed value

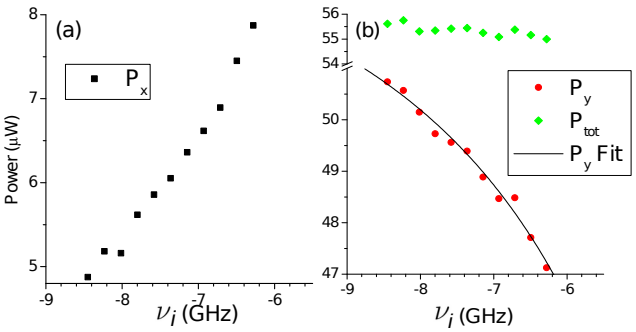

Fig. 5. Experimental values of (a) the power of x-polarization and (b) of y-polarization and total power , as a function of ν_i for $P_i = 151\ \mu W$ and $I = 3.05$ mA. Symbols correspond to experimental results. Solid line corresponds to the fit using Eq. (32).

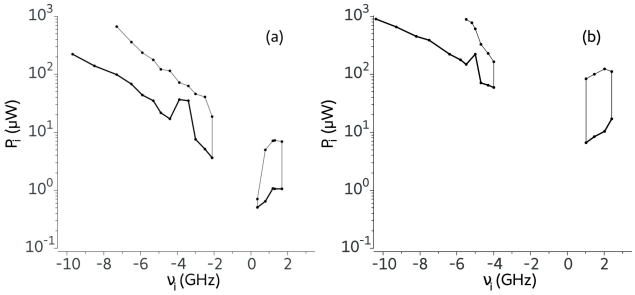

Fig. 6. Experimental values of the injected power for which IL+PS is observed as a function of ν_i , for (a) $I = 3$ mA, and (b) $I = 5$ mA. $P_{i,down}$ and $P_{i,up}$ are identified with thick and thin lines, respectively.

of ν_i, we have increased P_i from zero and have recorded the range of P_i in which IL+PS is observed in the optical spectrum. This process is repeated for several values of ν_i. The results are shown in Fig. 6(a) and Fig. 6(b) for $I = 3$ mA and $I = 5$ mA, respectively. Two regions in which IL+PS is observed appear at negative and positive values of ν_i. The region at positive ν_i appears at lower values of P_i than that observed at negative values of ν_i. These regions are bounded by two curves, $P_{i,down}$, and $P_{i,up}$, that correspond to the values of P_i at which IL+PS appears and disappears, respectively, when increasing P_i. For negative ν_i values $P_{i,up}$ monotonically decreases as ν_i increases. $P_{i,down}$ behaves similarly with the exception of a small region, -4.2 GHz $\leq \nu_i \leq -3$ GHz for Fig. 6(a) and -5.2 GHz $\leq \nu_i \leq -4.4$ GHz for Fig. 6(b). These regions corresponds to observation of period-2 dynamics in the x-polarization below the $P_{i,down}$ curve. Period-4 and chaotic dynamics in the x-polarization has also been observed close to this region and will be discussed elsewhere. This contrasts with all the other ν_i values in which IL+PS is observed, for which period-1 dynamics in the x-polarization, with a frequency given by ν_i, is always observed below $P_{i,down}$. Comparison between Fig. 6(a) and Fig. 6(b) shows that the left region of IL+PS extends to ν_i values closer to zero as I decreases. Also the region that appears at positive ν_i values shifts upwards to the right as I increases. Fig. 6(a) and Fig. 4(a) in [19] are obtained for the same device and very similar values of the bias current. We note that results are similar with the exception of a small region, -3.3 GHz $\leq \nu_i \leq -2.1$ GHz in which we now observe the IL+PS state. This new region has been obtained by making a more careful repetition of the measurements, correcting in this way results of Fig. 4(a) in [19].

4. THEORETICAL MODEL

We theoretically study the polarization dynamics of the VCSEL subject to parallel optical injection with the widely used spin-flip model (SFM) [24]. This is a rate equation model for the polarization modes of a single-mode VCSEL in which we introduce an injection term (to account for a linearly polarized optical injection in the direction of emission of the solitary VCSEL). The model equations are given in Eq. (1)-Eq. (4), where E_x and E_y are the two linearly polarized slowly varying components of the field in the x and y directions, and D and n are two carrier variables. D accounts for the total population inversion between conduction and valence bands, while n is the difference between the population inversions for the spin-up and spin-down radiation channels [25, 26].

$$\frac{dE_x}{dt} = -(\kappa+\gamma_a)E_x - i(\kappa\alpha+\gamma_p)E_x + \kappa(1+i\alpha)(DE_x + inE_y) + \kappa E_{inj}e^{i2\pi\nu_{inj}t} + \left(\sqrt{\frac{R_+}{2}}\xi_+(t) + \sqrt{\frac{R_-}{2}}\xi_-(t)\right) \quad (1)$$

$$\frac{dE_y}{dt} = -(\kappa-\gamma_a)E_y - i(\kappa\alpha-\gamma_p)E_y + \kappa(1+i\alpha)(DE_y - inE_x) + i\left(\sqrt{\frac{R_-}{2}}\xi_-(t) - \sqrt{\frac{R_+}{2}}\xi_+(t)\right) \quad (2)$$

$$\frac{dD}{dt} = -\gamma\left[D(1+|E_x|^2+|E_y|^2) - \mu + in(E_yE_x^* - E_xE_y^*)\right] \quad (3)$$

$$\frac{dn}{dt} = -\gamma_s n - \gamma\left[n(|E_x|^2+|E_y|^2) + iD(E_yE_x^* - E_xE_y^*)\right] \quad (4)$$

The normalized bias current is given by :

$$\mu = \frac{\tau_n}{\tau_e}\frac{\frac{I}{I_{th}} - 1}{1 - \frac{N_t}{N_{th}}} + 1 \quad (5)$$

where I and I_{th} are the current and threshold current, respectively, τ_n is the differential carrier lifetime at threshold ($\tau_n = 0.48$ ns), τ_e is the carrier lifetime at threshold ($\tau_e = 1.21$ ns), N_t and N_{th} are the carrier number at transparency and threshold, respectively, being $N_t = 9\times10^6$, and $N_{th} = 1.21\times10^7$ [27]. Other parameters are the field decay rate ($\kappa = 33\ ns^{-1}$), the linear dichroism ($\gamma_a = -0.21\ ns^{-1}$), the linewidth enhancement factor ($\alpha = 2.8$), the linear birefringence ($\gamma_p = 103.34\ ns^{-1}$), the decay rate of D ($\gamma = 2.08\ ns^{-1}$) and the spin-flip relaxation rate ($\gamma_s = 2100\ ns^{-1}$). E_{inj} is the amplitude of the injected light. ν_{inj} is the detuning between the frequency of the injected light and the intermediate frequency between those of the x and y polarization, ν_x and ν_y, where $2\pi\nu_x = \alpha\gamma_a - \gamma_p$ and $2\pi\nu_y = \gamma_p - \alpha\gamma_a$, and therefore $\nu_i = \nu_{inj} - \nu_x$. Spontaneous emission noise rates are included in Eqs. Eq. (1), Eq. (2) and are given $R_\pm = \beta_{SF}\gamma[(D\pm n) + G_N N_t/(2\kappa)]$, where β_{SF} accounts for the fraction of spontaneously emitted photons that are coupled into the laser mode and G_N is the differential gain ($G_N = 2.152\times10^4\ s^{-1}$). Fluctuations due to spontaneous emission are included in our calculations by $\xi_+(t)$ and $\xi_-(t)$ (complex Gaussian noise terms of zero mean and time correlation given by $<\xi_i(t)\xi_j^*(t')> = \delta_{ij}\delta(t-t')$).

We note that these parameters were extracted for a similar free-running VCSEL in previous work [25, 27].

5. THEORETICAL RESULTS

Theoretical optical spectra obtained by numerical integration of Eqs. Eq. (1)-Eq. (4) are shown in Fig. 7. These spectra correspond to the conditions of Fig. 3(d), $\nu_i = -5.88$ GHz and $I = 3.05$ mA. They have been obtained with an integration time step of 0.01 ps, a 5 ps sampling time and an average over 50 temporal windows of 327.68 ns duration after a transient of 80 ns. The optical spectrum corresponding to each linear polarization is plotted with a different colour. Fig. 7(a) shows the results obtained for a very small value of β_{SF}. These results illustrate the IL+PS state obtained when the deterministic version of our model is used. The behaviour is qualitatively similar to that shown in Fig. 3(d): locking of the parallel polarization mode to the optical injection and excitation of the free-running orthogonal polarization of the mode are observed. Fig. 7(b) shows that we obtain the same behaviour in our simulations when considering realistic levels of the strength of spontaneous emission noise, $\beta_{SF} = 6.5 \times 10^{-4}$ [25]. Spontaneous emission noise excites a small peak in the parallel emission at its free-running frequency, that can also be observed in Fig.3(d). Also noise excites satellite peaks around the main peaks of parallel and orthogonal polarizations. The frequency separation between the main and the satellite peaks in Fig. 7(b) is 2 GHz, that is close to the theoretical relaxation oscillation frequency $= (2\kappa\gamma(\mu-1))^{1/2}/2\pi = 2.1$ GHz. These peaks are not observed in Fig.3(d) because they are below the noise level: they are smaller than the peak of the parallel polarization at zero frequency, that is already barely visible in our experimental results of Fig.3(d). However we note that those corresponding to the orthogonal polarization mode can be observed under different injection conditions as it is shown in Fig. 1(d) of Ref. [19]. Also Fig. 7(b) shows some tiny satellite peaks that appear at -11.8, 27 and 39 GHz with a frequency separation of ν_i with respect to the main peaks.

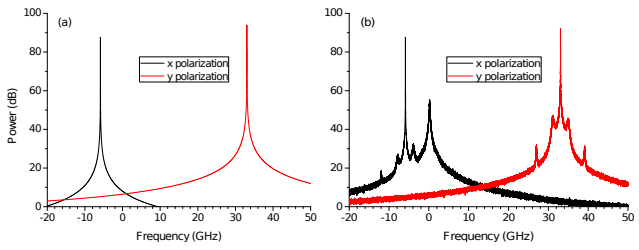

Fig. 7. Theoretical optical spectra when $\nu_i = -5.88$ GHz, $I = 3.05$ mA, $E_{inj} = 0.45$, for (a) $\beta_{SF} = 10^{-20}$, and (b) $\beta_{SF} = 6.5\ 10^{-4}$. Black (red) colour represents the parallel (orthogonal) polarization.

A simple analysis of the IL+PS solution can be performed when the spin-flip relaxation rate is very large, as it was measured for a similar device [25]. In this case the values of the variable n are very small [25]. We have checked this by integrating Eqs. Eq. (1)-Eq. (4) to obtain the range of variation of the n variable in the IL+PS state. Our results indicate that n oscillates around the zero value with $\nu_y - \nu_{inj}$ frequency but with a very small amplitude ($8\ 10^{-4}$ for the case illustrated in Fig. 7). Our approximation consists then in taking $n = 0$ in Eqs. Eq. (1)-Eq. (4) and write

$$E_x(t) = A_x(t)\ \exp\left(i(2\pi\nu_{inj}t + \phi_x(t))\right) \quad (6)$$

$$E_y(t) = A_y(t)\ \exp\left(i(2\pi\nu_y t + \phi_y(t))\right) \quad (7)$$

to obtain the following equations

$$\dot{A}_x = (\kappa(D-1) - \gamma_a)A_x + \kappa E_{inj}\cos\phi_x \quad (8)$$

$$\dot{A}_y = (\kappa(D-1) + \gamma_a)A_y \quad (9)$$

$$\dot{\phi}_x = \kappa\alpha(D-1) - 2\pi\nu_i - \alpha\gamma_a - \frac{\kappa E_{inj}}{A_x}\sin\phi_x \quad (10)$$

$$\dot{\phi}_y = \alpha(\kappa(D-1) + \gamma_a) \quad (11)$$

$$\dot{D} = -\gamma[D(1 + A_x^2 + A_y^2) - \mu] \quad (12)$$

The steady-state solution is found by solving the following equations

$$0 = (\kappa(D_0-1) - \gamma_a)A_{x,0} + \kappa E_{inj}\cos\phi_{x,0} \quad (13)$$

$$0 = (\kappa(D_0-1) + \gamma_a)A_{y,0} \quad (14)$$

$$0 = \kappa\alpha(D_0-1) - 2\pi\nu_i - \alpha\gamma_a - \frac{\kappa E_{inj}}{A_{x,0}}\sin\phi_{x,0} \quad (15)$$

$$0 = \alpha(\kappa(D_0-1) + \gamma_a) \quad (16)$$

$$0 = -\gamma\left[D_0(1 + A_{x,0}^2 + A_{y,0}^2) - \mu\right] \quad (17)$$

IL+PS state is characterized by $A_{x,0} > 0$, and $A_{y,0} > 0$. From Eq. (14) we obtain that

$$D_0 = 1 - \frac{\gamma_a}{\kappa} \quad (18)$$

since $A_{y,0} > 0$. This means that the total population inversion is fixed to a value that does not depend on $A_{x,0}$ nor $\phi_{x,0}$. In this way, the fact that the depressed polarization mode is lasing provides a simpler expression for the carrier density than when a single-polarization mode is considered for which $D_0 = 1 + \gamma_a/\kappa - E_{inj}\cos(\phi_{x,0})/A_{x,0}$, and $A_{x,0}$ is found solving a third-order equation also involving $\phi_{x,0}$.

From substitution of Eq. (18) in Eq. (13) and Eq. (15) we obtain that $\sin\phi_{x,0} = -2\gamma_a(\pi\nu_i/\gamma_a + \alpha)A_{x,0}/(\kappa E_{inj})$ and $\cos\phi_{x,0} = 2\gamma_a A_{x,0}/(\kappa E_{inj})$. From Eq. (17) and Eq. (18) we obtain that

$$P_x + P_y = \frac{\mu}{1 - \frac{\gamma_a}{\kappa}} - 1 \quad (19)$$

where $P_x = A_{x,0}^2$, and $P_y = A_{y,0}^2$ are the power of x and y polarizations, respectively. After some operations we also obtain

$$P_x = \left(\frac{\kappa}{2\gamma_a}\right)^2 \frac{P_{inj}}{1 + \left(\frac{\pi\nu_i}{\gamma_a} + \alpha\right)^2} \quad (20)$$

$$\phi_{x,0} = -\arctan\left(\frac{\pi\nu_i}{\gamma_a} + \alpha\right) \quad (21)$$

where $P_{inj} = E_{inj}^2$ is the power of the optical injection. Eq. (19) shows that the total power emitted by the VCSEL, $P_{tot} = P_x + P_y$ is constant and independent on P_{inj} and ν_i. The power of y-polarization, P_y, can be obtained by using Eq. (19) and Eq. (20) and its phase, $\phi_{y,0}$, can take any value since it does not appear in Eq. (13)-Eq. (17). Eq. (19) and Eq. (20) show that in the IL+PS solution both P_x and P_y depend linearly on P_{inj} in such a way

that the total power is constant. This is in agreement with our experimental results shown in Fig. 4.

The dependence of P_x, P_y and $\phi_{x,0}$ on ν_i is nonlinear and given by the previous equations. Fig. 8 shows P_x , P_y and $\phi_{x,0}$ as a function of ν_i obtained from Eq. (19)-Eq. (21) for an injected power similar to that of Fig. 7.

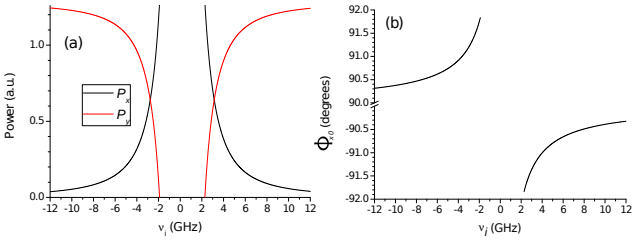

Fig. 8. Theoretical steady state values of (a) P_x, P_y and (b) $\phi_{x,0}$, as a function of ν_i for $I = 3.05$ mA and $E_{inj} = 0.45$.

We observe a region around zero frequency detuning in which solutions do not exist. This corresponds to the region in which P_y obtained from Eq. (19) and Eq. (20) becomes negative. P_x (P_y) decreases (increases) when $|\nu_i|$ increases. Experimental results shown in Fig. 5 are in qualitative agreement with Fig. 8(a). Fig. 8(b) shows that if $\nu_i < 0$ ($\nu_i > 0$) $\phi_{x,0}$ is in the second (third) quadrant and very close to 90° (-90°), as obtained from the expressions for $\sin\phi_{x,0}$ and $\cos\phi_{x,0}$.

IL+PS solution exists for a very wide range of ν_i. However, our experimental results of Fig. 5 and Fig. 6 indicate that it can only be observed in a range of a few GHz, providing that the injected power is fixed. A linear stability analysis of the IL+PS solution must be done in order to obtain theoretically under which conditions it can be observed. This analysis has been recently done in a two-polarization mode semiconductor laser [20] modelled by the dimensionless rate equations subject to TE-polarized optical injection

$$\frac{dE_1}{ds} = (1+i\alpha)NE_1 + \overline{\gamma}e^{i\Delta s} \quad \textbf{(22)}$$

$$\frac{dE_2}{ds} = (1+i\alpha)\overline{\kappa}(N-\beta)E_2 \quad \textbf{(23)}$$

$$T\frac{dN}{ds} = P - N - (1+2N)\left(|E_1|^2 + |E_2|^2\right) \quad \textbf{(24)}$$

where E_1, E_2, and N are the amplitude of the TE electric field, the amplitude of the TM electric field, and carrier density, respectively. s is the time, T is the ratio of carrier to cavity lifetimes, P is the pump parameter, $\overline{\gamma}$ is the injection strength, Δ is the frequency detuning between the injected signal and the solitary laser, $\overline{\kappa}$ is the ratio of the gain coefficients of the TM and TE modes, and β measures the losses of the TM mode compared to the TE mode. The TE (TM) mode corresponds to the x (y) polarization mode because if we make the following change of variables in Eq. (1)-Eq. (4) with $n = 0$, $E_x = \sqrt{2}E_1\exp(-i(\gamma_p - \alpha\gamma_a)t)$, $E_y = \sqrt{2}E_2\exp(i(\gamma_p - \alpha\gamma_a)t)$, $D = (2N+1)(1+\gamma_a/\kappa)$, and $t = s/(2\kappa(1+\gamma_a/\kappa))$ we obtain Eq. (22)-Eq. (24) with :

$$T = \frac{2\kappa}{\gamma}\left(1+\frac{\gamma_a}{\kappa}\right) \quad \textbf{(25)}$$

$$P = \frac{\mu}{2\left(1+\frac{\gamma_a}{\kappa}\right)} - \frac{1}{2} \quad \textbf{(26)}$$

$$\overline{\gamma} = \frac{E_{inj}}{2\sqrt{2}\left(1+\frac{\gamma_a}{\kappa}\right)} \quad \textbf{(27)}$$

$$\Delta = \frac{\pi\nu_i}{\kappa\left(1+\frac{\gamma_a}{\kappa}\right)} \quad \textbf{(28)}$$

$$\beta = -\frac{\gamma_a}{\kappa\left(1+\frac{\gamma_a}{\kappa}\right)} \quad \textbf{(29)}$$

and $\overline{\kappa} = 1$. The Routh-Hurwitz conditions for the stability of the TE+TM steady-state solution can be applied to the IL+PS state by using Eq. (25)-Eq. (29), and Eqs. (18)-(20) of Ref. [20]. Fig. 9 shows with solid and black lines the Hopf bifurcations from the two-mode steady state (H_2 lines in [20]) that are obtained with our VCSEL parameters. Also the bifurcation from the two-mode solution from the pure-mode solution (SB_2 line in [20]) is shown with a red line. SB_2 line is obtained as follows. If we use $P_y \geq 0$ in Eq. (19) and Eq. (20) we obtain

$$P_{inj} \leq \left[\frac{2\gamma_a}{\kappa}\right]^2\left[\frac{\mu}{1-\frac{\gamma_a}{\kappa}} - 1\right]\left[1+\left(\frac{\pi\nu_i}{\gamma_a}+\alpha\right)^2\right] \quad \textbf{(30)}$$

SB_2 line is obtained when the equal sign holds in Eq. (30). Eq. (30) also means that the IL+PS state must be below the SB_2 line in Fig. 9. Two different bias currents, similar to those in Fig. 6, are considered in Fig. 9. Also, two different values of γ_a, -0.21 ns^{-1} and -0.36 ns^{-1}, have been considered in Fig. 9(a) and Fig. 9(b), respectively. A different value has been considered for 5 mA because γ_a depends on the bias current [25, 28]. Fig. 9(a) and Fig. 9(b) show two regions, at positive and negative ν_i, in which the TE+TM steady state, that is the IL+PS state, is stable. The left part of the region that appears at positive ν_i is closed by the SB_2 line, as in [20]. Comparison between Fig. 6 and Fig. 9 shows that good qualitative agreement is found between experiments and theory.

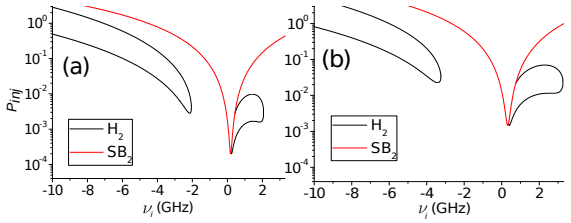

Fig. 9. Theoretical values of the injected power for which IL+PS is stable as a function of ν_i, for (a) $I = 3$ mA, and (b) $I = 5$ mA. Hopf bifurcations from the two-mode steady state (H_2) and bifurcation to the two-mode solution from the pure-mode solution (SB_2) are shown with black and red lines, respectively.

We now analyse the dependence of the previous diagrams on the value of γ_a. Fig. 10(a) shows the results for a bias current value of 3 mA and three different values of γ_a. We have plotted

only the part of SB_2 that closes the region that appears at positive ν_i. We distinguish with thick (thin) lines in Fig. 10(a) the lower (upper) boundaries of the regions, $P_{inj,down}$ ($P_{inj,up}$). $P_{inj,down}$ ($P_{inj,up}$) is calculated when $a_1a_2a_3 - a_3^2 - a_1^2a_4$ becomes positive (negative) as P_{inj} is increased, where a_1 to a_4 are defined in Eq. (19) of [20].

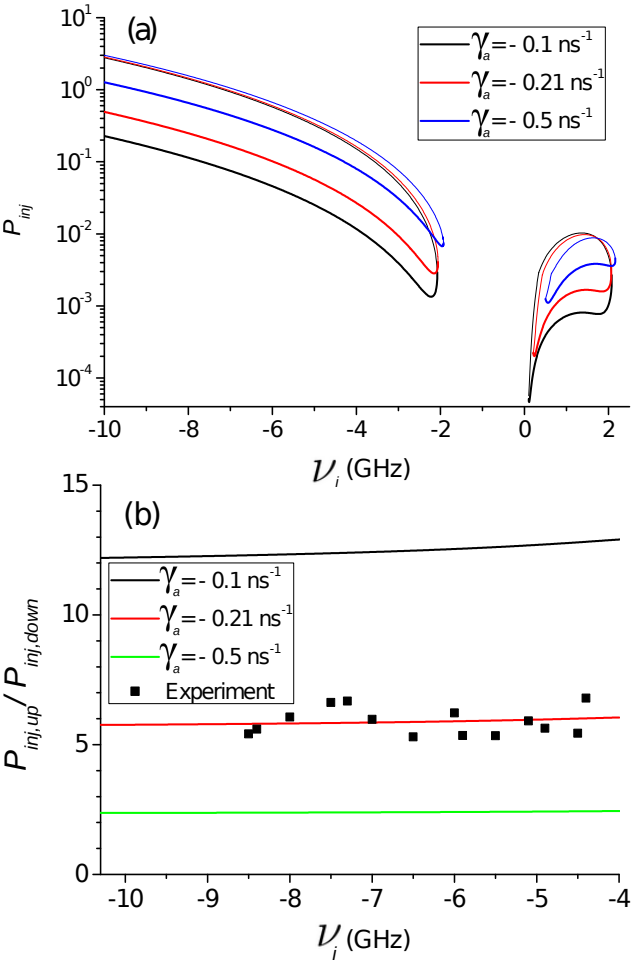

Fig. 10. (a) Theoretical values of the injected power for which IL+PS is stable as a function of ν_i ($P_{inj,down}$ and $P_{inj,up}$ are identified with thick and thin lines, respectively). (b) Theoretical and experimental values of $P_{inj,up}/P_{inj,down}$ as a function of ν_i. In these figures several values of γ_a are considered and $I = 3$ mA.

Fig. 10(a) shows that for large and negative values of ν_i, $P_{inj,up}$ is almost independent on γ_a in contrast to $P_{inj,down}$ that increases as $|\gamma_a|$ increases. This means that as the y-mode of the solitary VCSEL is more suppressed with respect to the corresponding x-mode the stability region of IL+PS narrows, similarly to what was found in [20] when β increases. Fig. 10(b) shows the ratio $P_{inj,up}/P_{inj,down}$ obtained with the curves of Fig. 10(a) for negative values of ν_i. The value of this ratio is almost independent on ν_i providing that $|\nu_i|$ is large enough. For instance $P_{inj,up}/P_{inj,down}$ only changes 3% from $\nu_i = -10$ GHz to $\nu_i = -5$ GHz when $\gamma_a = -0.21$ ns^{-1}. The value of $P_{inj,up}/P_{inj,down}$ mainly depends on the value of γ_a in such a way that increases as $|\gamma_a|$ decreases.

An approximate expression for $P_{inj,up}/P_{inj,down}$ can be derived by evaluating the roots of $a_1a_2a_3 - a_3^2 - a_1^2a_4 = 0$ at large and negative values of ν_i . We obtain that

$$\frac{P_{inj,up}}{P_{inj,down}} \simeq \frac{\gamma\mu}{4|\gamma_a|} \tag{31}$$

This simple expression gives the value shown in Fig. 10(b) at $\nu_i = -10$ GHz with a relative error of 2.3, 1.5 and 0.6% for $\gamma_a = -0.1$, -0.21 and -0.5 ns^{-1}, respectively. Fig. 10(b) also shows the experimental values of $P_{i,up}/P_{i,down}$ obtained for $I = 3$ mA. Very good agreement is found between our experimental and theoretical results when $\gamma_a = -0.21$ ns^{-1}, so this is the value that we have been considering in our calculations for $I = 3$ mA. We have followed the same procedure for $I = 5$ mA and we have found a value of $\gamma_a = -0.36$ ns^{-1}, that is the one we used in Fig. 9(b). Measurement of $P_{i,up}/P_{i,down}$ and Eq. Eq. (31) constitute a simple way of extracting the γ_a parameter of a VCSEL.

We can also check some of our simple expressions, for instance those giving the dependence of the power of both linear polarizations as a function of ν_i, Eq. (19) and Eq. (20). If we consider the conversion factors, c_t and c_x such that $\mathbf{P_{tot}} = c_t P_{tot}$ and $\mathbf{P_x} = c_x P_x$, the measured power emitted by the VCSEL in the y-polarization, $\mathbf{P_y}$, can be fitted by the following expression

$$P_y = A - \frac{B}{1 + \left(\frac{\pi\nu_i}{\gamma_a} + \alpha\right)^2} \tag{32}$$

We have made a two-parameters (A, B) fit of the experimental points corresponding to $\mathbf{P_y}$ in Fig. 5(b) using Eq. (32) with $\gamma_a = -0.21$ ns^{-1}, and $\alpha = 2.8$. Results corresponding to our best fit ($A = 55.1 \pm 0.3$ μW, $B = 7.4\ 10^4 \pm 3\ 10^3$ μW, and $\overline{R}^2 = 0.984$) are plotted in Fig. 5(b) with a solid line. Good agreement for the frequency detuning dependence is found between our theoretical and experimental results.

6. DISCUSSION AND CONCLUSIONS

The IL+PS state is unusual because optical injection in the polarization with smaller optical losses causes emission in the polarization with larger losses. For values of the injected power, P_{inj}, smaller than $P_{inj,down}$ period-1 dynamics in the x linear polarization is observed [19]. As P_{inj} is increased the IL+PS may become stable while this period-1 solution destabilizes [19]. The region of stability of the IL+PS state shrinks when β, or equivalently $|\gamma_a|$, increases. The Routh-Hurwitz stability conditions give an upper bound for the presence of a stable IL+PS, $\beta \leq \beta_c = (-1 + \sqrt{1 + 4(1 + 2P)/T})/4$ [20]. The linear dichroism must satisfy $\gamma_a \geq -\beta_c\kappa/(1 + \beta_c)$ if we want an unsupported polarization mode (y) activated by injecting light into the natural supported mode (x). For our VCSEL parameters this conditions reads $\gamma_a \geq -1.09$ ns^{-1} for a 3 mA bias current.

Some mismatch of the frequency detuning range in which IL+PS appears can be observed in Fig. 5 ($\nu_i \leq -6.3$ GHz) and in Fig. 6(a) ($\nu_i \leq -5.1$ GHz for $P_i = 151\mu$W). This can be explained because there is bistability between the IL+PS and x-polarized injection locked solutions [19]. Bistability between the injection locked (single-mode) and a two-color equilibrium state (steady state) has been also observed in a two-color laser [21]. Mismatch is observed because Fig. 5(a) has been obtained decreasing ν_i with fixed P_i while Fig. 6(a) was obtained by increasing P_i with fixed values of ν_i. Also some discrepancy can be observed between the experimental shape of $P_{i,down}$ (Fig. 6(a))and the

theoretical shape of $P_{inj,down}$ (Fig. 9(a)). Again this discrepancy can be explained by the bistability that we experimentally find between the IL+PS and the x-polarized period-2 solution that appears below the bump of $P_{i,down}$ in Fig. 6(a). This bump is observed when increasing P_i with fixed values of ν_i. However, when P_i is decreased from IL+PS region with fixed values of ν_i, $P_{i,down}$ follows the monotonous dependence on ν_i observed in Fig. 9(a). Also some examples of nonlinear dynamics (period-1 and period-2) involving both linear polarizations have been observed [19]. Polarization bistability and nonlinear dynamics found in single-mode VCSELs under parallel optical injection will be the subject of future work. Our VCSEL is characterized by a large γ_s parameter value in the framework of SFM. This explains the good agreement with the theory for $n = 0$. We have checked our results for smaller values of γ_s. For instance, results shown in Fig. 7(a) are maintained if $\gamma_s \geq 250$ ns^{-1}. Smaller values of the γ_s parameter ($\gamma_s = 240$ ns^{-1}) result in the excitation of only the parallel polarization mode with periodic dynamics with a frequency close to $|\nu_i|$.

As mentioned in the introduction there are several differences between the IL+PS and the TME states[21–23], being the excitation of two linear polarizations in IL+PS the most relevant from the physical point of view. In IL+PS, observed in single-mode lasers, optical injection close to the lasing mode makes the other linear polarization mode to appear. However in TME, observed in two-mode lasers, optical injection only produces locking of one mode to the injection leaving the other longitudinal mode with the same linear polarization unchanged. Eqs. (22)-(25) are not equivalent to the model used to analyze TME because we consider that the two polarization modes differ in loss ($\beta > 0$) while ($\beta = 0$) in [21–23] and because nonlinear cross and self saturation terms are used in [21–23]. Just the introduction of a small β parameter changes the steady states that can be observed in both models without optical injection. In our case $\beta > 0$ means that there are only two steady states. The first one, in which $|E_1|^2 = P$, $|E_2|^2 = 0$, and $N = 0$ is stable because a linear stability analysis gives the following eigenvalues: $-\beta$ and $\lambda_\pm = \left(-(1+2P) \pm i\sqrt{8PT - (1+2P)^2}\right)/(2T)$. The second one, $|E_1|^2 = 0$, $|E_2|^2 = (P-\beta)/(1+2\beta)$, $N = \beta$ is unstable. In [21–23] $\beta = 0$ means that infinite steady states can be observed such that $0 \leq |E_1|^2 \leq P$, $|E_2|^2 = P - |E_1|^2$, $N = 0$. If the steady state with $|E_1|^2 = P$, $|E_2|^2 = 0$, and $N = 0$ is chosen its linear stability properties are different to those of our stable state because the eigenvalues obtained with the model of [21–23] are 0 and $\lambda_\pm$.

Summarizing, we have analyzed in detail the IL+PS state that appears in a single-transverse mode VCSEL when subject to parallel optical injection. We have obtained simple analytical expressions that describe the amplitude and phase of the electrical fields of both linear polarizations. These expressions show that the power of both linear polarizations depend linearly on the injected power for a fixed frequency detuning between the injected light and the parallel linear polarization of the VCSEL. A simple nonlinear dependence between the power of both linear polarizations and the frequency detuning has been found. We have also obtained that the total power emitted by the VCSEL is constant and independent on the injected optical power and on the frequency detuning. We have checked these results experimentally for different frequency detunings and bias currents. We have obtained experimental and theoretical stability maps in the injected power-frequency detuning plane identifying the regions in which the state is obtained. We have measured and calculated maps for different bias currents with good qualitative agreement. We have obtained that the ratio between the injected powers corresponding to the upper and lower boundaries of these maps is independent on the frequency detuning providing this is large and negative. We have also analysed the dependence of the theoretical maps on the linear dichroism. A very simple analytical expression that describes that ratio has been derived providing a simple method to extract the linear dichroism of the device.

7. ACKNOWLEDGMENTS

This work has been funded by the Ministerio de Economía y Competitividad (MINECO/FEDER, UE), Spain under project TEC2015-65212-C3-1-P. A. Quirce acknowledges FWO for her Post Doc fellowship and H. Thienpont and K. Panajotov are grateful to the Methusalem foundation for financial support. M. Sciamanna acknowledges the support of Préfecture de Lorraine and SGAR through the PHOTON project (FEDER) and the APOLLO (FEDER/FNADT) project. Y. Hong acknowledges the support of the Ser Cymru National Research Network in Advanced Engineering and Materials.

REFERENCES

1. R. Lang, "Injection locking properties of a semiconductor laser," IEEE Journal of Quantum Electronics **18**, 976–983 (1982).
2. G. Van Tartwijk and D. Lenstra, "Semiconductor lasers with optical injection and feedback," Quantum and Semiclassical Optics: Journal of the European Optical Society Part B **7**, 87 (1995).
3. S. Wieczorek, B. Krauskopf, T. Simpson, and D. Lenstra, "The dynamical complexity of optically injected semiconductor lasers," Physics Reports **416**, 1–128 (2005).
4. T. Simpson, J. Liu, A. Gavrielides, V. Kovanis, and P. Alsing, "Period-doubling cascades and chaos in a semiconductor laser with optical injection," Physical review A **51**, 4181 (1995).
5. J. Ohtsubo, *Semiconductor lasers: stability, instability and chaos*, vol. 111 (Springer, 2012).
6. M. Sciamanna and K. A. Shore, "Physics and applications of laser diode chaos," Nature Photonics **9**, 151–162 (2015).
7. R. Michalzik, *VCSELs: fundamentals, technology and applications of vertical-cavity surface-emitting lasers*, vol. 166 (Springer, 2012).
8. F. Koyama, "Recent advances of vcsel photonics," Journal of Lightwave Technology **24**, 4502–4513 (2006).
9. C.-H. Chang, L. Chrostowski, and C. J. Chang-Hasnain, "Injection locking of vcsels," IEEE Journal of selected topics in quantum electronics **9**, 1386–1393 (2003).
10. M. Virte, K. Panajotov, H. Thienpont, and M. Sciamanna, "Deterministic polarization chaos from a laser diode," Nature Photonics **7**, 60–65 (2013).
11. Z. G. Pan, S. Jiang, M. Dagenais, R. A. Morgan, K. Kojima, M. T. Asom, R. E. Leibenguth, G. D. Guth, and M. W. Focht, "Optical injection induced polarization bistability in vertical-cavity surface-emitting lasers," Applied physics letters **63**, 2999–3001 (1993).
12. Y. Hong, K. Shore, A. Larsson, M. Ghisoni, and J. Halonen, "Polarisation switching in a vertical cavity surface emitting semiconductor laser by frequency detuning," IEE Proceedings-Optoelectronics **148**, 31–34 (2001).
13. T. Mori, Y. Yamayoshi, and H. Kawaguchi, "Low-switching-energy and high-repetition-frequency all-optical flip-flop operations of a polarization bistable vertical-cavity surface-emitting laser," Applied Physics Letters **88**, 101102 (2006).
14. J. B. Altés, I. Gatare, K. Panajotov, H. Thienpont, and M. Sciamanna, "Mapping of the dynamics induced by orthogonal optical injection in vertical-cavity surface-emitting lasers," IEEE journal of quantum electronics **42**, 198–207 (2006).
15. K. H. Jeong, K. H. Kim, S. H. Lee, M. H. Lee, B.-S. Yoo, and K. A. Shore, "Optical injection-induced polarization switching dynamics in 1.5-

m wavelength single-mode vertical-cavity surface-emitting lasers," IEEE Photonics Technology Letters **20**, 779–781 (2008).
16. R. Al-Seyab, K. Schires, N. A. Khan, A. Hurtado, I. D. Henning, and M. J. Adams, "Dynamics of polarized optical injection in 1550-nm vcsels: theory and experiments," IEEE Journal of Selected Topics in Quantum Electronics **17**, 1242–1249 (2011).
17. A. A. Qader, Y. Hong, and K. A. Shore, "Role of suppressed mode in the polarization switching characteristics of optically injected vcsels," IEEE Journal of Quantum Electronics **49**, 205–210 (2013).
18. M. Nizette, M. Sciamanna, I. Gatare, H. Thienpont, and K. Panajotov, "Dynamics of vertical-cavity surface-emitting lasers with optical injection: a two-mode model approach," JOSA B **26**, 1603–1613 (2009).
19. A. Quirce, P. Pérez, A. Popp, Á. Valle, L. Pesquera, Y. Hong, H. Thienpont, and K. Panajotov, "Polarization switching and injection locking in vertical-cavity surface-emitting lasers subject to parallel optical injection," Optics letters **41**, 2664–2667 (2016).
20. G. Friart, A. Gavrielides, and T. Erneux, "Analytical stability boundaries of an injected two-polarization semiconductor laser," Physical Review E **91**, 042918 (2015).
21. S. Osborne, K. Buckley, A. Amann, and S. O'Brien, "All-optical memory based on the injection locking bistability of a two-color laser diode," Optics express **17**, 6293–6300 (2009).
22. A. Amann, *Nonlinear laser dynamics: from quantum dots to cryptography. K. Lüdge (Ed). Chapter 10* (John Wiley & Sons, 2012).
23. D. O'Shea, S. Osborne, N. Blackbeard, D. Goulding, B. Kelleher, and A. Amann, "Experimental classification of dynamical regimes in optically injected lasers," Optics express **22**, 21701–21710 (2014).
24. J. Martin-Regalado, F. Prati, M. San Miguel, and N. Abraham, "Polarization properties of vertical-cavity surface-emitting lasers," IEEE Journal of Quantum Electronics **33**, 765–783 (1997).
25. P. Pérez, A. Valle, and L. Pesquera, "Polarization-resolved characterization of long-wavelength vertical-cavity surface-emitting laser parameters," JOSA B **31**, 2574–2580 (2014).
26. P. Pérez, A. Quirce, A. Valle, A. Consoli, I. Noriega, L. Pesquera, and I. Esquivias, "Photonic generation of microwave signals using a single-mode vcsel subject to dual-beam orthogonal optical injection," IEEE Photonics Journal **7**, 1–14 (2015).
27. P. Pérez, A. Valle, I. Noriega, and L. Pesquera, "Measurement of the intrinsic parameters of single-mode vcsels," Journal of Lightwave Technology **32**, 1601–1607 (2014).
28. M. Van Exter, M. Willemsen, and J. Woerdman, "Polarization fluctuations in vertical-cavity semiconductor lasers," Physical Review A **58**, 4191 (1998).